How to Cite: Galiyeva, A.R., Aseyev, V.O., Bardadym, Y.V., Zhumagaliyeva, T.S., Borsynbayev, A.S., & Tazhbayev, Y.M. (2026) Isoniazid-Loaded PEGylated Albumin Nanoparticles: Development and Taguchi Optimization. *Eurasian Journal of Chemistry*. https://doi.org/10.31489/2959-0663/4-26-5

Article

Received: 22 September 2026 | Revised: 18 November 2026 |
Accepted: 20 November 2026 | Published online: 27 November 2026

UDC 541.64

https://doi.org/10.31489/2959-0663/4-26-5

Aldana R. Galiyeva[1]*, Vladimir O. Aseyev[2], Yuliia V. Bardadym[2],
Tolkyn S. Zhumagaliyeva[1], Askhat S. Borsynbayev[1], Yerkeblan M. Tazhbayev[1]

[1]*Buketov Karaganda National Research University, Karaganda, Kazakhstan*
[2]*Department of Chemistry, University of Helsinki, Helsinki, Finland*
*(*Corresponding author's e-mail: aldana_karaganda@mail.ru)*

Isoniazid-Loaded PEGylated Albumin Nanoparticles: Development and Taguchi Optimization

Tuberculosis remains a serious global health problem, which emphasizes the need to improve delivery systems for existing anti-tuberculosis drugs. The aim of this study was to develop nanoparticles based on bovine serum albumin (BSA) modified with polyethylene glycol (PEG) and containing isoniazid (INH), as well as to optimize the conditions for their preparation. The nanoparticles were synthesized using PEG activated with dichloro-s-triazine (PEGTC2) by desolvation followed by cross-linking with glutaraldehyde. The Taguchi orthogonal array method was used to evaluate the influence of seven formulation and process parameters, including the molecular weight and concentration of PEGTC2, BSA and INH concentrations, pH, ethanol addition rate, and stirring rate. The optimized nanoparticles were characterized by an average size of 227 ± 1 nm, a polydispersity index (PDI) of 0.026 ± 0.002, a zeta potential of −26 ± 2 mV, an encapsulation efficiency (EE) of 94%, and a nanoparticle yield of 43%. Analysis by scanning electron microscopy (SEM) showed that the nanoparticles were predominantly spherical, and In vitro release studies showed a gradual release of isoniazid from the nanoparticles, reaching approximately 2.3 mg after 24 h. These results support further study of PEGylated albumin nanoparticles as nanocarriers for the sustained delivery of isoniazid.

Keywords: isoniazid, PEGylated albumin nanoparticles, bovine serum albumin, activated poly(ethylene glycol), Taguchi design, nanoparticle optimization, tuberculosis, desolvation method, drug delivery, orthogonal array.

Introduction

Tuberculosis, caused by *Mycobacterium tuberculosis* (MTB), remains one of the most pressing infectious disease challenges in modern public health. According to the World Health Organization, approximately 10.7 million people contracted tuberculosis in 2024, and the number of deaths was approximately 1.23 million [1]. An additional problem is the drug resistance of MTB, particularly multidrug-resistant tuberculosis (MDR-TB), in which the pathogen is resistant to at least isoniazid and rifampicin [2-4]. The duration of treatment, the need to use multiple drugs, and the risk of side effects underscore the importance of exploring new approaches to improving the efficacy and safety of antituberculosis therapy.

The use of nanostructured drug delivery systems is a promising area of research. Nanoparticles make it possible to modify the pharmacokinetic properties of drugs, ensure their controlled release, increase stability, and facilitate more effective delivery of the drug directly to the site of infection [5-8]. Albumin-based nanoparticles are of particular interest due to their biocompatibility, biodegradability, and albumin's ability to interact with various drug compounds [9-11]. However, the efficacy of albumin nanoparticles depends largely on their surface characteristics and colloidal stability. PEGylation is widely used to increase surface hy-

© 2026 The Authors. This is an open access article under the CC BY-NC-ND license (http://creativecommons.org/licenses/by-nc-nd/4.0/)

drophilicity, reduce nanoparticle aggregation, and improve colloidal stability [12-16]. Various PEG derivatives, including activated PEG, have been employed for protein modification [17-19]. In this context, dichloro-s-triazine-activated PEG (PEGTC2) represents a promising approach for the production of PEG-modified albumin nanoparticles.

The properties of albumin nanoparticles also depend to a large extent on composition and process parameters, including the molecular weight and concentration of PEG, the concentration of albumin and the drug, the pH value, the rate of desolvation agent addition, and mixing conditions. The traditional optimization method, based on sequentially changing parameters, does not fully account for the combined effect of multiple composition variables and requires a large number of experiments. Taguchi's experimental design method provides a systematic approach to simultaneously evaluating the influence of multiple factors with a limited number of experiments, thereby enabling the identification of conditions for producing nanoparticles with specified physicochemical characteristics [20-22].

Despite significant interest in albumin-based drug delivery systems, the systematic development and optimization of PEGylated BSA NPs loaded with isoniazid and prepared using PEG activated with dichloro-s-triazine have not been sufficiently studied. Therefore, the aim of this study was to develop PEGylated BSA nanoparticles containing isoniazid (PEGTC2–BSA–INH NPs) and to systematically optimize their preparation process using a Taguchi orthogonal design. The effects of factors such as PEG molecular weight and concentration, BSA and isoniazid concentrations, medium pH, ethanol addition rate, and stirring rate on the nanoparticle characteristics were investigated. The scientific novelty of this study lies in the systematic seven-factor Taguchi optimization of the PEGTC2–BSA–INH nanoparticle system, for which the combined effects of key formulation and process parameters have not previously been investigated. The nanoparticles obtained during the optimization process were comprehensively characterized to assess their potential as sustained-release isoniazid nanocarriers.

Experimental

Materials

Poly(ethylene glycol) (PEG) with molecular weights of 4000 and 6000 Da, bovine serum albumin (BSA, lyophilized powder, purity 98%), isoniazid (INH; IUPAC name: pyridine-4-carbohydrazide, purity >99%) and 2,4,6-Trichloro-1,3,5-triazine (cyanuric chloride) were purchased from Sigma-Aldrich (Germany). Ethanol (90%) was supplied by Dosfarm (Kazakhstan), while a 50% glutaraldehyde solution was obtained from CJSC Kupavnareaktiv (Staraya Kupavna, Russia). Phosphate-buffered solution (PBS) was prepared using sodium hydrogen phosphate and potassium dihydrogen phosphate supplied by JSC Reatex (Moscow, Russia).

Synthesis of Polyethylene Glycol Dichloro-s-Triazine ("Activated PEG")

Polyethylene glycol (PEG, MW 4000 or MW 6000) was dissolved in anhydrous benzene (200 mL) and then cooled to 10°C (Figure 1). Cyanuric chloride (a fivefold molar excess, dissolved in benzene) was slowly added to the PEG solution, followed by anhydrous sodium carbonate (a fivefold molar excess). The reaction mixture was stirred at room temperature for 24 hours, and then the solid inorganic salt was filtered off from the solution. An excess of 40/60 petroleum ether was added to the filtrate, and the "Activated PEG" derivative precipitated as a white solid. The precipitate was collected, dissolved in benzene (200 mL), and precipitated again with 40/60 petroleum ether. This process was repeated twice to remove unreacted cyanuric chloride and obtain a pure intermediate.

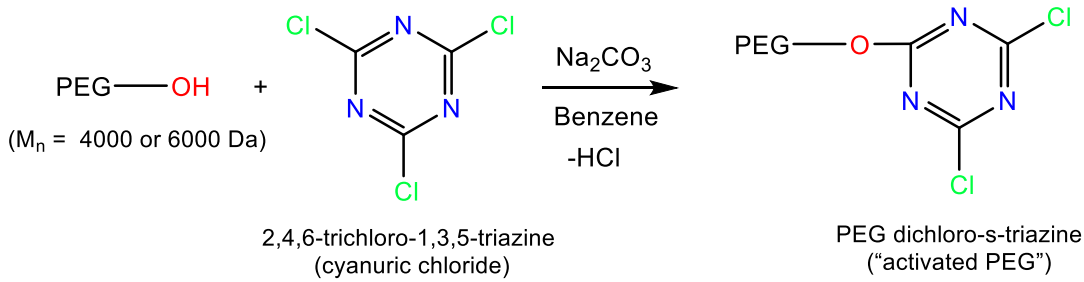

Figure 1. Schematic representation of the proposed synthesis of activated PEG using cyanuric chloride.

Preparation of PEGTC2–BSA–INH NPs

PEG-modified albumin nanoparticles were prepared by the desolvation method [19, 23, 24], based on protein precipitation induced by the gradual addition of a water-miscible organic solvent. BSA (20 or 40 mg/mL) and activated PEG (MW of 4000 or 6000 Da, at concentration 10 or 20 mg/mL) were dissolved in distilled water, and the pH of the resulting solution was adjusted to 6 or 7 using 0.5 M HCl or 0.2 M NaOH, respectively. The resulting solution was treated with ultrasound for 3 minutes (Launch Tech, Shenzhen, China) with a nominal power rating of 100 W and an operating frequency of 28 kHz. Isoniazid was then dissolved directly in the 3 mL of BSA and PEG solution to obtain a final INH concentration of 4 or 6 mg/mL. Particles were obtained by adding 9 mL of ethanol as a desolvating agent to the BSA and PEG solution (ethanol addition rate of 1 or 2 mL/min) while stirring (200 or 300 rpm) at room temperature. The resulting particles were stabilized by adding 8% glutaraldehyde as a cross-linking agent (1.175 μL/mg BSA), followed by stirring for 24 hours. An 8% glutaraldehyde solution, freshly prepared by diluting the commercial 50% glutaraldehyde solution with distilled water, was used for nanoparticle crosslinking. The nanoparticle suspension was centrifuged at 13,150 × g for 20 min using a MiniSpin centrifuge (Eppendorf, Hamburg, Germany). Following synthesis, the PEGTC2–BSA–INH NPs were collected by centrifugation and washed repeatedly with distilled water to remove unbound PEG, free INH, and residual water-soluble impurities. The pellet was collected and dried.

The Taguchi method was used to optimize the PEGylation of bovine albumin nanoparticles loaded with isoniazid. In this study, a standard L8 orthogonal array was used to investigate a seven-factor system at two levels, as shown in Table 1. The molecular weight and concentration of PEGTC2, BSA concentration, pH, INH concentration, ethanol addition rate, and stirring rate were selected as formulation and process factors, while particle size, PDI, zeta potential, encapsulation efficiency (EE), and NPs yield were evaluated as response variables.

The type and concentration of PEGTC2, the concentration of BSA, pH, the concentration of INH, the ethanol addition rate, and the stirring rate were selected as factors affecting the particle size and PDI of PEGTC2–BSA–INH nanoparticles.

Table 1

Experimental parameters and Taguchi L8 levels for the preparation of PEGTC2–BSA–INH nanoparticles

Category	Name	Units	Level 1	Level 2
A	MW of PEGTC2	Da	4000	6000
B	[PEGTC2]	mg/mL	10	20
C	[BSA]	mg/mL	20	40
D	pH	–	6	7
E	[INH]	mg/mL	4	6
F	Ethanol addition rate	mL/min	1	2
G	Stirring rate	rpm	200	300

Particle Size Distribution, Zeta Potential, and Morphological Characterization of PEGTC2–BSA–INH NPs

The hydrodynamic diameter and polydispersity index (PDI) of PEGTC2–BSA–INH NPs were evaluated by dynamic light scattering (DLS) with a Zetasizer Nano S90 (Malvern Instruments Ltd., Malvern, UK). Before the measurements, the nanoparticle dispersions were appropriately diluted with distilled water. Surface charge was characterized by measuring the zeta potential using electrophoretic light scattering on a Zetasizer Nano ZS90 (Malvern Instruments Ltd., Worcestershire, UK). For zeta potential measurements, the prepared nanoparticles were dispersed in distilled water without additional pH adjustment. The measurements were performed at the natural pH of the aqueous dispersion. The exact pH values of the dispersions at the time of zeta potential analysis were not determined. The pH values of 6 and 7 reported in Table 2 refer exclusively to the nanoparticle synthesis conditions. The morphology of the dried nanoparticles was visualized by scanning electron microscopy (SEM) using a MIRA 3LM microscope (TESCAN, Brno, Czech Republic).

Encapsulation Efficiency and Yield of PEGTC2–BSA–INH NPs

The encapsulation of INH within PEGTC2–BSA–INH NPs was assessed using an indirect approach based on the amount of free drug remaining in the supernatant following centrifugation. Unencapsulated INH was quantified by high-performance liquid chromatography (HPLC) on a Shimadzu LC-20 Prominence system (Shimadzu, Kyoto, Japan). The obtained HPLC data were subsequently used to determine the encapsulation efficiency (EE), while the nanoparticle yield was calculated from the mass of the recovered nanoparticles according to the Equations 1-2 below:

$$\mathrm{EE}(\%) = \frac{m_{INH,total} - m_{INH,free}}{m_{INH,total}} \times 100\% \quad (1)$$

$$\text{NPs Yield}(\%) = \frac{\mathrm{m}_{NPs}}{m_{INH} + m_{BSA} + m_{\mathrm{PEGTC2}}} \times 100\% \quad (2)$$

where $\mathrm{m}_{\mathrm{INH,total}}$ – is the initial total mass of INH; $\mathrm{m}_{\mathrm{INH,free}}$ – is the mass of unencapsulated INH determined in the supernatant; $\mathrm{m}_{\mathrm{NPs}}$ – is the mass of the dried nanoparticles; $\mathrm{m}_{\mathrm{INH}}$, $\mathrm{m}_{\mathrm{BSA}}$ and $\mathrm{m}_{\mathrm{PEGTC2}}$ – are the initial masses of INH, BSA, and PEGTC2 used for nanoparticle preparation, respectively.

In vitro Study of Isoniazid Release from PEGTC2–BSA–INH NPs

The release behavior of INH from PEGTC2–BSA–INH NPs under in vitro conditions was evaluated by a dialysis technique. Dried nanoparticles (27 mg) were suspended in 3 mL of PBS (pH 7.4), placed in a dialysis membrane with a molecular weight cut-off (MWCO) of 1 kDa, and immersed in 14 mL of PBS (pH 7.4) as the external release medium. The experiment was carried out at 37 °C in a water bath. At specified sampling times, 1 mL of the external medium was withdrawn, and the amount of released INH was quantified by HPLC. The cumulative drug release was calculated using the following Equation 3:

$$\text{Drug release}(\%) = \frac{\mathrm{m}_{INH,released}}{\mathrm{m}_{INH\ in\ NPs}} \times 100\% \quad (3)$$

where $\mathrm{m}_{INH,released}$ is the mass of INH released into the medium and $\mathrm{m}_{INH\ in\ NPs}$ is the mass of INH encapsulated in the nanoparticles.

Nuclear Magnetic Resonance (NMR) Characterization of PEG and Activated PEG Derivatives

The structural characteristics of the starting PEG and its activated derivatives (PEGTC2, molecular weights of 4000 and 6000 Da) were investigated using ^{1}H and ^{13}C NMR spectroscopy on a Bruker AV 400 spectrometer. The starting PEG was dissolved in D_2O, whereas the activated PEG derivatives were analyzed in DMF-d_7. The ^{1}H and ^{13}C NMR spectra were acquired using 10 and 512 scans, respectively.

Thermal Characterization of PEGTC2–BSA–INH NPs by Thermogravimetric Analysis and Differential Scanning Calorimetry

Thermal properties of INH, BSA, PEGTC2 and dried PEGTC2–BSA–INH NPs were characterized by TGA and DSC (LabSYS evo TGA/DTA/DSC system, Setaram, France). Each sample was subjected to controlled heating from 30 to 600 °C at a rate of 10 °C/min. Measurements were performed under a nitrogen atmosphere maintained at a flow rate of 30 mL/min.

Fourier-Transform Infrared Spectroscopy of PEGTC2–BSA–INH NPs

FTIR analysis was performed to examine the structural features of the INH, BSA, PEGTC2 and the resulting PEGTC2–BSA–INH NPs. Spectra were acquired with an FSM 1202 FTIR spectrometer (Infraspek Ltd., Russia). For sample preparation, 3 mg of the analyzed material was homogenized with 100 mg of KBr and subsequently pressed into a pellet. Measurements were carried out within the 4000-400 cm^{-1} wavenumber region using a spectral resolution of 8 cm^{-1}.

Toxicity Assessment Using Artemia salina Nauplii

The preliminary toxicity of the samples was assessed using an Artemia salina nauplius survival test. Artemia salina cysts were incubated in artificial seawater at 25 °C for 48 hours to produce nauplii. The study was conducted in vitro using two-day-old nauplii. The samples were tested at concentrations of 0.1, 0.5 and 1mg/mL; three independent replicates were carried out for each concentration. Using a Pasteur pipette, ten

nauplii were placed into each vial containing the relevant sample. The vials were kept at room temperature in the light for 24 hours. At the end of the incubation period, the number of surviving and dead nauplii was counted, and the survival rate was calculated as the percentage of surviving individuals out of the total number of nauplii used in the experiment.

Statistical Analysis

Experimental measurements were conducted in triplicate (n = 3), with the results expressed as mean ± standard deviation (SD). Mean values and standard deviations were calculated using Minitab 19 software. The effects of the investigated formulation and process parameters on nanoparticle characteristics were evaluated by analysis of variance (ANOVA) using Design-Expert software. Statistical analysis of the toxicity data was performed using one-way ANOVA, followed by Tukey's post hoc test for multiple comparisons. Differences were considered statistically significant at $p < 0.05$.

Results and Discussion

PEGylation of proteins is a clinically proven approach to increasing the half-life and reducing the immunogenicity of protein therapies [25-27]. PEGylation increases the apparent molecular weight of proteins, provides steric shielding of the protein surface, and can improve their pharmacokinetic and pharmacodynamic profiles [27].

Preliminary experiments were carried out using non-activated PEG for the PEGylation of BSA-INH nanoparticles. To this end, PEG was first mixed with an aqueous solution of BSA, after which isoniazid and ethanol were added. The resulting formulations were then crosslinked using glutaraldehyde. The PEG-BSA-INH nanoparticles had a mean particle size of 612.2 ± 58.9 nm and a PDI of 0.607 ± 0.090. The dispersion exhibited low colloidal stability, as evidenced by an increase in particle size and PDI over a 30-minute period. Furthermore, solvent evaporation led to the formation of a cream-like mass, which prevented the isolation of individual nanoparticles. These results demonstrated that non-activated PEG is unsuitable for the preparation of stable and homogeneous PEGylated BSA–INH nanoparticles using the desolvation method with glutaraldehyde as a crosslinking agent under the conditions studied. Therefore, to produce PEGylated albumin nanoparticles with desirable physicochemical characteristics, it was necessary to investigate the structure of albumin and suitable methods for PEG attachment.

PEGylated proteins are typically obtained by covalent conjugation of activated PEG to reactive groups on the protein, including the side chains of lysine, cysteine, histidine, arginine, aspartic acid, glutamic acid, serine, threonine, and tyrosine, as well as the N- and C-terminal groups [16, 27]. Therefore, to successfully PEGylate albumin, PEG was activated prior to nanoparticle preparation. The synthesis of polyethylene glycol dichloro-s-triazine (PEGTC2) was carried out according to previously reported methods [28,29] using cyanuric chloride.

The structural characteristics of the starting PEG and its derivatives obtained following activation with cyanuric chloride were investigated using ^{1}H and ^{13}C NMR spectroscopy (Figure S1). The spectra of the starting PEG were recorded in D_2O, whereas the activated PEG derivatives with molar masses of 4000 and 6000 g/mol (PEG4 and PEG6, respectively) were analyzed in DMF-d_7.

The ^{1}H NMR spectrum of the starting PEG exhibited characteristic resonances of the methylene protons (–CH_2–CH_2–O–) at 3.62 ppm [30]. Similar signals were observed in the spectra of PEG4 and PEG6, indicating the preservation of the polyethylene glycol backbone following the activation procedure.

The ^{13}C NMR spectrum of the starting PEG exhibited an intense resonance at $\delta = 69.47$ ppm, corresponding to the methylene carbon atoms of the polyethylene glycol backbone. In the spectra of the activated PEG derivatives (PEG4 and PEG6), this signal shifted slightly to $\delta = 70.38$ ppm. This variation may reflect changes in the chemical environment of the polymer chains following the activation procedure. However, the influence of the different solvents used for NMR analysis cannot be excluded. Characteristic ^{13}C NMR resonances of substituted triazine rings may occur in the δ 160–175 ppm region, depending on their chemical structure [31]. Although signals near 162 ppm were observed in the spectra of PEG4 and PEG6, their overlap with the characteristic resonances of DMF-d_7 prevented unambiguous assignment to triazine carbon atoms [32]. The degree of PEG activation and the number of dichloro-s-triazine groups introduced per PEG molecule were not quantitatively determined in the present study.

PEGylated bovine albumin nanoparticles were prepared using "activated PEG" via the desolvation method, as described above. Desolvation was performed with ethanol, and the nanoparticles were cross-

linked with glutaraldehyde. The scheme for the preparation of PEGTC2–BSA–INH NPs is shown in Figure 2.

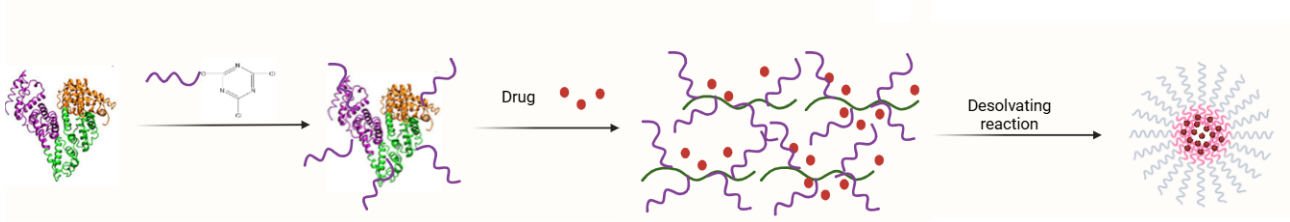

Figure 2. Scheme for the production of PEGTC2–BSA–INH NPs

Isoniazid was loaded in situ into the PEGTC2–BSA nanoparticles during particle formation. To optimize the formulation and process conditions, a Taguchi L8 orthogonal array was employed to systematically evaluate the effects of PEGTC2 molecular weight and concentration, BSA and INH concentrations, pH, ethanol addition rate, and stirring rate. The resulting formulations were characterized in terms of particle size, PDI, zeta potential, EE, and nanoparticle yield. The experimental design and corresponding physicochemical characteristics of the obtained PEGTC2–BSA–INH NPs are summarized in Table 2.

Table 2

Taguchi L8 orthogonal array and physicochemical characteristics of PEGTC2–BSA–INH NPs obtained under different formulation and process conditions

No	A: MW of PEGTC2, Da	B: [PEGTC2], mg/mL	C: [BSA], mg/mL	D: pH	E: [INH], mg/mL	F: Ethanol addition rate, mL/min	G: Stirring rate, rpm	Average particle size, nm	PDI	Zeta potential, mV	EE, %	NPs yield, %
1	4000	10	20	7	6	2	300	256±7	0.134±0.009	-25±1	77	41
2	6000	20	20	7	4	1	300	243±1	0.073±0.017	-47±1	70	39
3	6000	10	40	6	6	1	300	575±10	0.798±0.052	-27±5	86	37
4	4000	20	40	6	4	2	300	504±11	0.646±0.048	-30±2	89	21
5	4000	20	40	7	6	1	200	296±5	0.105±0.010	-31±2	83	31
6	6000	20	20	6	6	2	200	623±9	0.857±0.065	-13±2	89	36
7	4000	10	20	6	4	1	200	966±6	0.976±0.042	-23±3	83	33
8	6000	10	40	7	4	2	200	245±3	0.096±0.019	-16±3	86	51

The use of the Taguchi L8 experimental design revealed substantial effects of formulation and process conditions on nanoparticle characteristics of PEG–BSA–INH NPs (Table 2). The average particle size ranged from 243 ± 1 to 966 ± 6 nm, and the PDI ranged from 0.073 ± 0.017 to 0.976 ± 0.042, indicating that the nanoparticle formation process is strongly dependent on the selected combination of factors. The formation of particles smaller than 300 nm is desirable due to their potentially favorable characteristics for drug delivery applications [33, 34]. In all formulations prepared at pH 7, particles smaller than 300 nm with a PDI ≤ 0.134 were formed, whereas formulations prepared at pH 6 were characterized by significantly larger particle sizes and a broader size distribution. This suggests that pH was an important parameter determining the formation and stabilization of albumin NPs under the conditions studied. The EE remained relatively high for all formulations (70–89 %), despite significant differences in particle size and PDI values. The nanoparticle yield ranged from 21 to 51 %; the highest value was obtained in Experiment No. 8, which was also characterized by a small particle size (245 ± 3 nm) and a low PDI (0.096 ± 0.019). The zeta potential of PEGTC2–BSA–INH nanoparticles ranged from −13 ± 2 to −47 ± 1 mV (Table 2), indicating a negative surface charge across all formulations, primarily associated with ionized carboxyl groups of BSA [35, 36]. Variations in zeta potential may arise from changes in BSA–PEG interactions and the accessibility of surface ionizable groups. PEG molecular weight and concentration may affect the position of the hydrodynamic slipping plane, while synthesis pH may influence BSA conformation and surface charge distribution [37–39].

The effects of the investigated factors on nanoparticle characteristics were evaluated using Design-Expert software, followed by analysis of variance (ANOVA) to identify statistically significant effects. Although the values of zeta potential, EE, and nanoparticle yield varied during the experiments, an analysis of variance revealed no statistically significant effect of the studied factors on these parameters ($p > 0.05$). Therefore, the detailed statistical analysis presented below focuses on particle size and the PDI — parame-

ters for which a significant effect was observed. The ANOVA tables for average size and polydispersity are presented in Table 3.

Table 3

ANOVA for the selected factorial model

Source	Sum of Squares	Degree of freedom	Mean Square	F-value	p-value	
(a) Size, nm						
Model	8.419×10^{-7}	4	2.105×10^{-7}	11.42	0.0368	significant
B-[PEGTC2]	2.894×10^{-10}	1	2.894×10^{-10}	0.0157	0.9082	
C-[BSA]	1.065×10^{-9}	1	1.065×10^{-9}	0.0578	0.8255	
D-pH	8.351×10^{-7}	1	8.351×10^{-7}	45.32	0.0067	
E-[INH]	5.441×10^{-9}	1	5.441×10^{-9}	0.2953	0.6246	
Residual	5.528×10^{-8}	3	1.843×10^{-8}			
(b) PDI						
Model	0.4582	4	0.1145	89.12	0.0019	significant
B-[PEGTC2]	0.0046	1	0.0046	3.55	0.1559	
C-[BSA]	0.0031	1	0.0031	2.38	0.2205	
D-pH	0.4483	1	0.4483	348.81	0.0003	
E-[INH]	0.0022	1	0.0022	1.73	0.2802	
Residual	0.0039	3	0.0013			

When the raw data were analyzed using ANOVA, the results showed that PEGTC2 molecular weight did not significantly affect the average particle size or PDI. The ethanol addition rate and stirring rate were treated as process noise factors. Their effects on particle size and PDI were not statistically significant under the investigated conditions. Therefore, these factors were not included in the ANOVA analysis. Consequently, the final models were based on factors B, C, D, and E.

Particle size data were transformed using the equation: $y' = (y + k)^{\lambda}$, where $k = 0$ and $\lambda = -1.25$. For the mean particle size (Table 3a), the ANOVA demonstrated that the model was statistically significant ($F = 11.42$, $p = 0.0368$). The predicted R^2 (0.56) was lower than the adjusted R^2 (0.86), with a difference greater than 0.2, indicating limited agreement between the two values. Nevertheless, the Adeq Precision value of 7 exceeded the recommended threshold of 4, indicating an adequate signal for exploring the design space.

For PDI, the data were transformed according to the equation $y' = (y + k)^{\lambda}$, where $k = 0$ and $\lambda = 0.34$. The resulting model was statistically significant ($F = 89.12$, $p = 0.0019$) (Table 3b). The close agreement between the predicted (0.94) and adjusted (0.98) R^2 values indicated satisfactory predictive performance of the model. In addition, an Adeq Precision of 19 confirmed a sufficient signal-to-noise ratio for navigation within the experimental design space.

The influence of the selected formulation variables on nanoparticle size and PDI is illustrated in Figure 3. Among the studied conditions, smaller particle sizes and lower PDI values were associated with pH 7 and an INH concentration of 4 mg/mL.

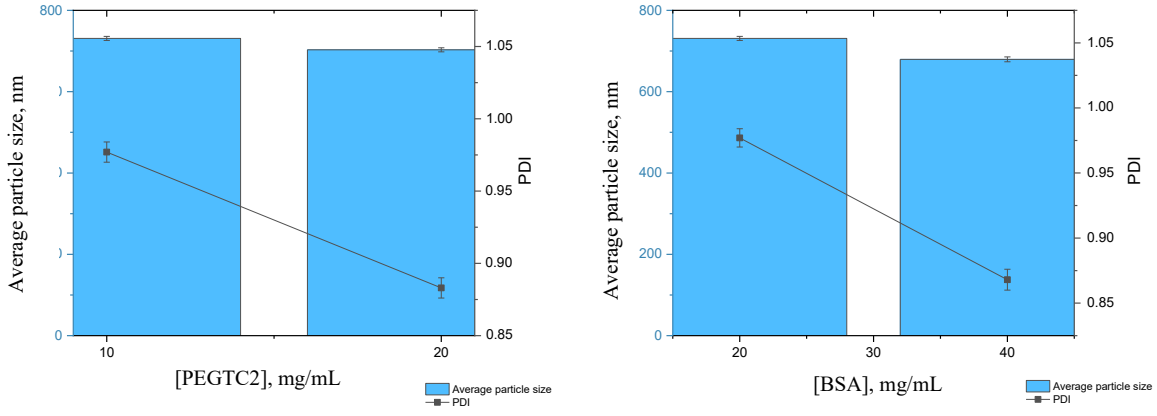

(a) (b)

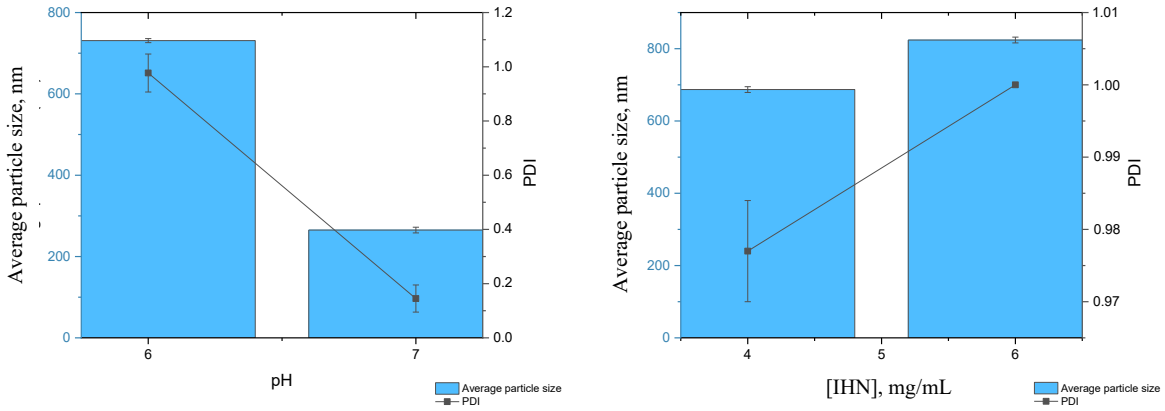

Figure 3. Influence of selected formulation factors on the mean particle size and PDI of PEG–BSA–INH NPs: (a) PEGTC2 concentration, (b) BSA concentration, (c) pH, and (d) INH concentration.

Based on the ANOVA results, particle size and PDI were selected as the primary responses for process optimization, while zeta potential, EE, and NPs yield were considered as auxiliary formulation constraints (Table 4).

Table 4

Optimal conditions for the synthesis of PEGTC2–BSA–INH NPs

Name	Goal	Lower Limit	Upper Limit	Lower Weight	Upper Weight
A:MW of PEGTC2	is equal to 6000	4000	6000	1	1
B:[PEGTC2]	is in range	10	20	1	1
C:[BSA]	is in range	20	40	1	1
D:pH	is equal to 7	6	7	1	1
E:[INH]	is equal to 4	4	6	1	1
F:Ethanol addition rate	is equal to 1	1	2	1	1
G:Stirring rate	is equal to 200	200	300	1	1
Size	minimize	243	966	1	1
PDI	minimize	0.073	0.976	1	1
Zeta potential	maximize	–47	–13	1	1
EE	maximize	70	89	1	1
NPs yield	maximize	21	51	1	1

Based on the ANOVA results, numerical optimization was performed using Design-Expert software, with particle size and PDI selected as the primary responses. A desirability function was applied to identify the combination of formulation and process parameters that minimized both responses [40]. Solution 2, with an overall desirability of 70 %, was selected for experimental verification. The selected formulation contained PEGTC2 with a molecular weight of 6000 Da at a concentration of 20 mg/mL, BSA at 40 mg/mL, and INH at 4 mg/mL and was prepared at pH 7, with an ethanol addition rate of 1 mL/min and a stirring rate of 200 rpm. The experimentally obtained particle size showed good agreement with the predicted value, whereas the PDI was lower than predicted, indicating a more homogeneous particle size distribution. Despite some differences between the predicted and experimental values, the results were considered acceptable within the scope of the model's predictions; the overall desirability value was 70 % (Table 5).

Table 5

Predicted and experimental results for PEGTC2–BSA–INH NPs

	Size, nm	PDI	Zeta potential, mV	EE, %	NPs yield, %
Predicted	252±5	0.069±0.018	-35±13	81	35
Experimental	227±1	0.026±0.002	-26±2	94	43
Error (%)	10	62	26	16	23

The morphology of the resulting nanoparticles was determined using SEM, as shown in Figure 4. SEM images revealed predominantly spherical nanoparticles, and the average diameter, calculated from the SEM data, was approximately 187 nm. This value was lower than the hydrodynamic diameter determined by DLS (227 ± 1 nm), which can be attributed to the solvation layer surrounding the nanoparticles in suspension, whereas SEM measures the size of particles in the dried state.

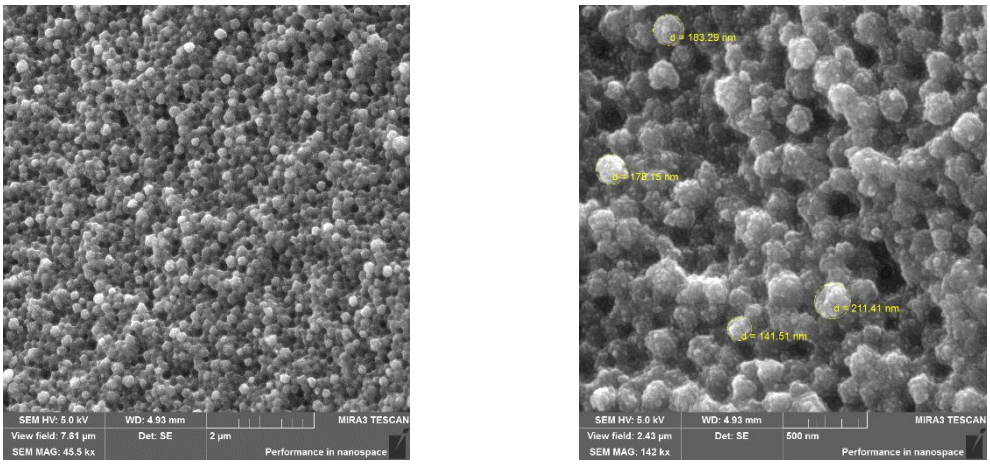

(a) (b)

Figure 4. SEM images of optimized PEGTC2–BSA–INH nanoparticles at two magnifications: (a) scale bar, 2 µm; (b) scale bar, 500 nm

The thermal stability of the samples was evaluated by TGA and DSC (Figure 5). During the initial heating stage, a slight increase in the INH and BSA mass was observed. In a nitrogen atmosphere, this behavior can be explained by the effect of temperature on buoyancy effect and by baseline drift, which may occur due to changes in the density of the purge gas and the response of the thermobalance during the heating process [41-43]. The DSC thermogram of isoniazid exhibited a pronounced endothermic peak at 177.2 °C, corresponding to its melting point, followed by a second endothermic event at 345.6 °C, which was attributed to thermal decomposition. The corresponding mass loss occurred over the temperature range of 250–430 °C and reached approximately 72 % [44-46]. In the case of BSA, the DSC thermogram revealed a three-step thermal degradation profile. The first endothermic event, observed at 98.9 °C, was associated with the evaporation of bound or residual moisture, whereas the subsequent thermal events at 227.3 and 313 °C were attributed to the degradation of the protein structure, primarily involving disruption of amide bonds [47,48]. The endothermic peak of PEGTC2 at approximately 60 °C was attributed to a phase transition, as no mass loss is observed. Mass loss occurs primarily in the range of 325–445 °C and 245–440 °C for PEGTC2 with MWs of 4000 and 6000 Da, respectively. This weight loss indicates thermal decomposition or evaporation within the material.

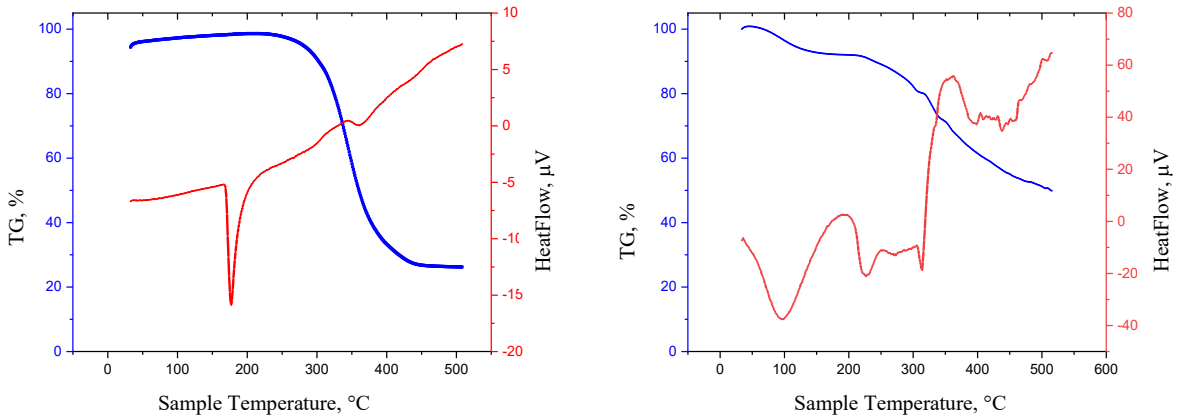

(a) (b)

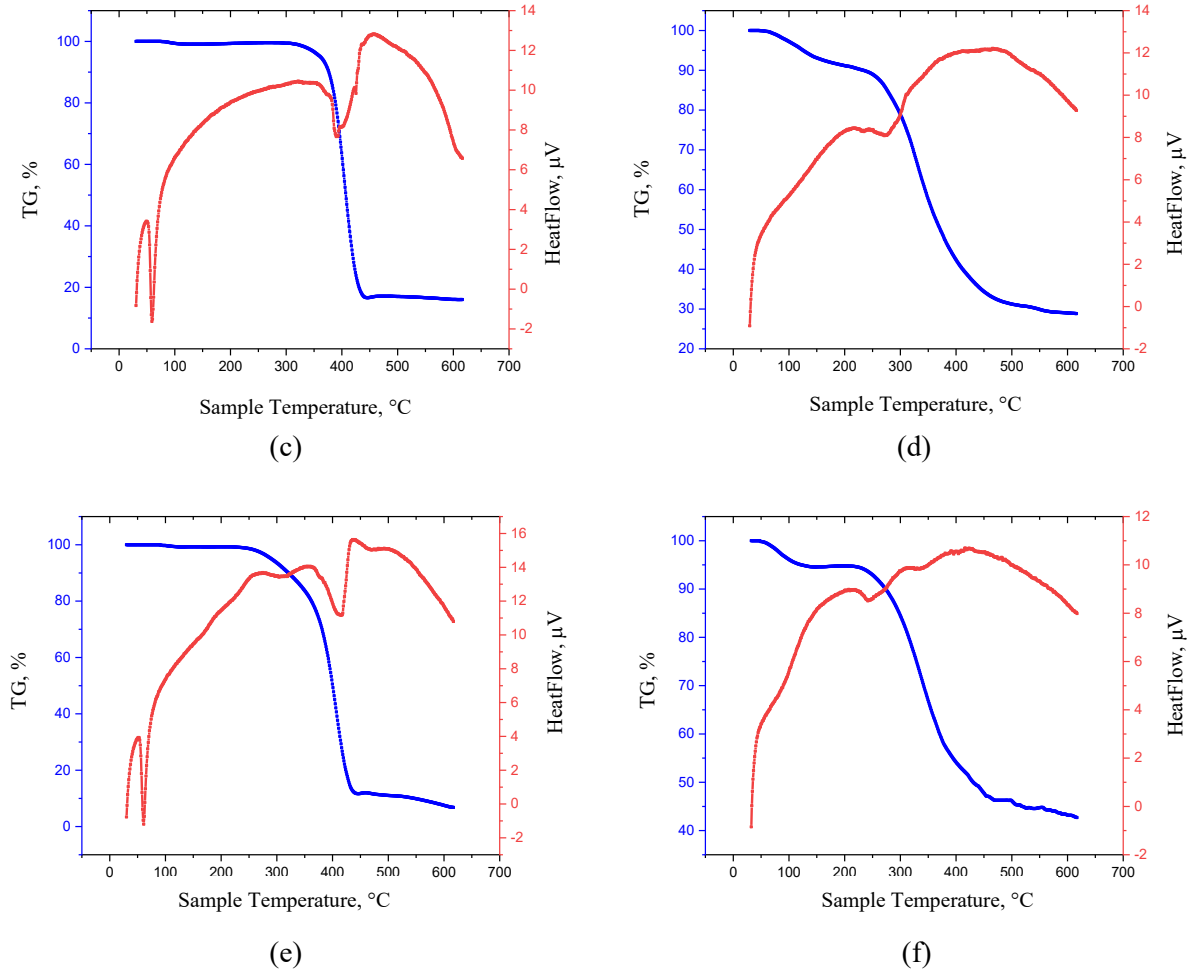

Figure 5. TGA and DSC curves for pure (a) isoniazid, (b) bovine serum albumin, (c), (e) poly(ethylene glycol) dichloro-s-triazine and (d), (f) PEGTC2–BSA–INH NPs with different MW of PEGTC2.

Figure 6 shows that substantial mass loss was observed in PEG-stabilized albumin NPs between 216 °C and 230 °C. At temperatures up to 100 °C, the weight loss is attributed to the evaporation of bound and residual water, consistent with the DSC measurements mentioned above. In a nitrogen atmosphere at 600 °C, the observed weight loss in PEGTC2 4000 and PEGTC2 6000 is 84 % and 93 %, respectively, while the weight loss in PEGylated NPs is 57 % and 71 % at this temperature (600 °C). Thus, the differences in weight loss between PEGTC2 and PEGTC2–BSA–INH were determined to be 27 % and 22 %, respectively.

To confirm the attachment of PEG to the albumin molecule and the incorporation of isoniazid, IR spectroscopy was used (Figure 6). The spectrum of pure INH exhibited the characteristic absorption bands associated with its functional groups. Pure INH displayed a broad FTIR band centered at approximately 3306 cm^{-1}, corresponding to N-H stretching, together with a distinct absorption at 1667 cm^{-1} assigned to the carbonyl (C=O) vibration of the hydrazide group [46,49]. The fingerprint region contained additional signals characteristic of INH, including vibrations associated with C=N, C-N, and N-N bonds. In the BSA spectrum, the typical absorption features of the protein structure were observed. A broad band around 3440 cm^{-1} was associated with O-H stretching, while the characteristic amide I and amide II bands appeared at 1647 and 1540 cm^{-1}, respectively. These bands arise predominantly from C=O stretching (amide I) and a combination of N-H bending and C-N stretching vibrations (amide II). A weaker band in the 1245 cm^{-1} region can be assigned to amide III vibrations [48,50,51]. The presence of these characteristic amide bands confirms the protein structure of BSA.

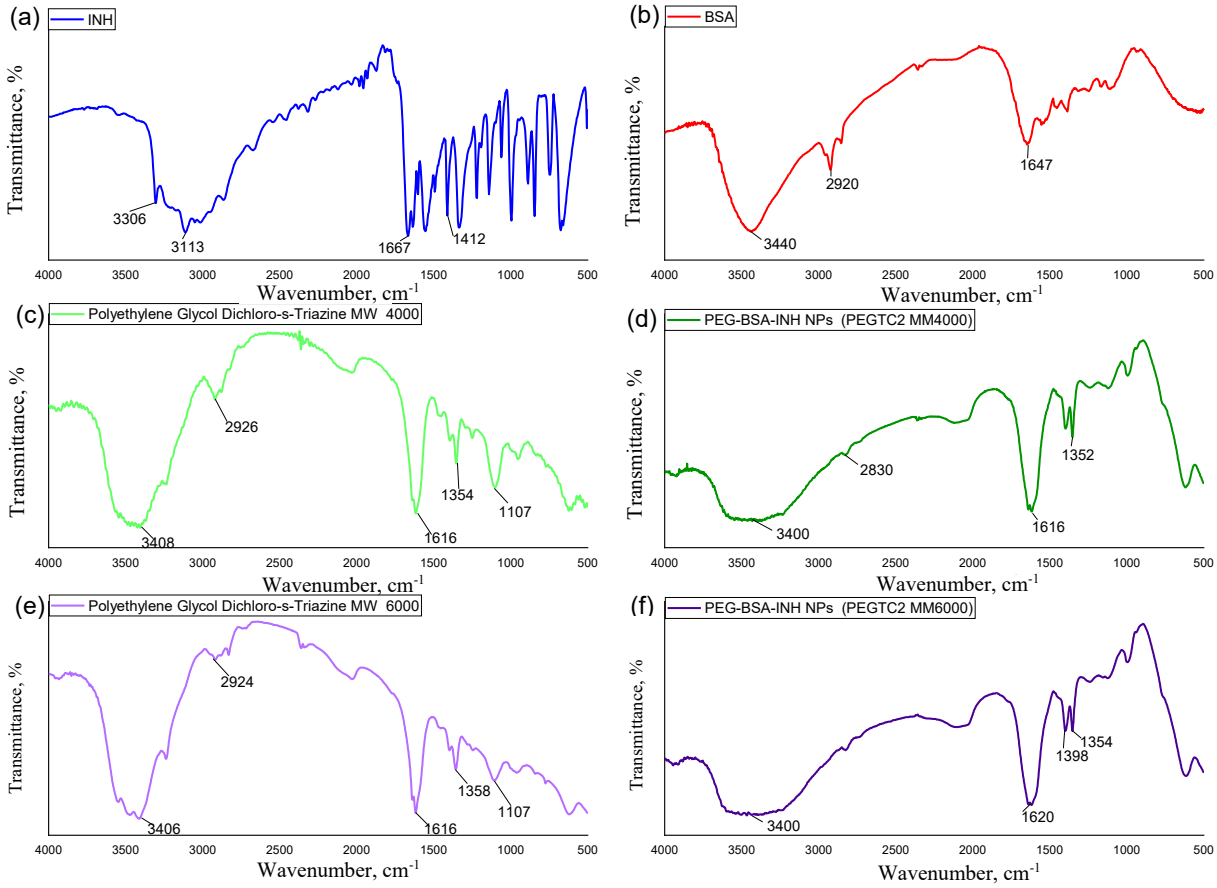

Figure 6. Fourier-transform infrared spectra of (a) pure isoniazid, (b) bovine serum albumin, (c), (e) Polyethylene Glycol Dichloro-s-Triazine and (d), (f) PEGTC2–BSA–INH NPs with different MW of PEGTC2

The FTIR spectra of PEGTC2 with molecular weights of 4000 and 6000 Da exhibited characteristic absorption bands at 3440 cm^{-1}, associated with O-H stretching vibrations, 2926 cm^{-1} corresponded to C-H stretching vibrations, 1354 cm^{-1}, associated with CH_2 bending vibrations, and 1107 cm^{-1}, assigned to C-O stretching vibrations. Compared with the spectrum of the starting PEG, the activated PEG exhibited an additional band at 1616 cm^{-1}, which was attributed to vibrations of the triazine ring [17,24,52,53]. The FTIR spectra of PEGTC2–BSA–INH NPs prepared using PEGTC2 with MW of 4000 and 6000 Da exhibited a broad absorption band at approximately 3400 cm^{-1}, attributed mainly to N-H and O-H stretching vibrations. The bands observed at 1398 and 1616 cm^{-1} were assigned to CH_2 vibrations and vibrations of the triazine ring of activated PEG, respectively. Thus, the IR spectroscopy results confirm the incorporation of PEG-dichloro-s-triazine and isoniazid molecules into albumin NPs.

The in vitro release behavior of INH from PEGTC2–BSA–INH NPs was evaluated in PBS at pH 7.4. The concentration of INH released into the medium was determined by HPLC, and the cumulative drug release was calculated as described above. The resulting release profile is presented in Figure 7.

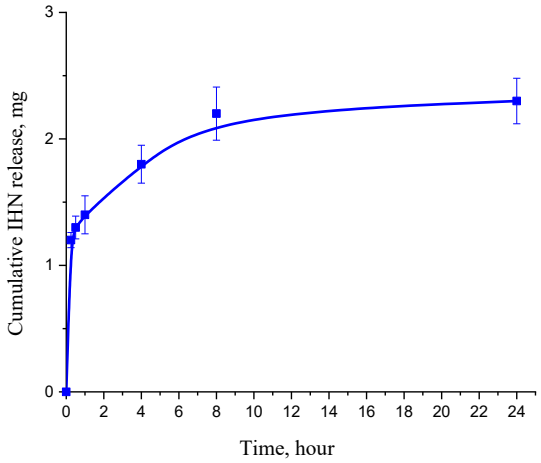

Figure 7. Cumulative isoniazid release from a polymer matrix of PEGTC2–BSA–INH NPs

The amount of INH released gradually increased during the experiment, reaching approximately 2.3 mg after 24 h. Thus, most of the encapsulated drug remained associated with the nanoparticles over the investigated period. The resulting profile confirms the ability of PEGTC2-BSA nanoparticles to provide prolonged release of isoniazid.

Encapsulating drugs within polymeric nanoparticles may help to reduce drug toxicity by modulating drug release, thereby minimizing the exposure to the free drug. Furthermore, PEGylation can enhance the colloidal stability of the albumin nanoparticles and may improve their biocompatibility [13, 19]. Although PEGylation is generally associated with reduced toxicity, previous studies have reported that PEG modification may also induce adverse biological effects depending on the PEG structure, molecular weight, and formulation characteristics [54, 55]. Therefore, the effect of PEGylation on nanoparticle toxicity cannot be assumed to be uniformly beneficial. In this context, the preliminary toxicity of PEGTC2–BSA–INH nanoparticles were evaluated using an Artemia salina nauplii survival assay and compared with that of non-PEGylated BSA–INH nanoparticles and Actinomycin D. Actinomycin D, a known cytotoxic agent, was included as a positive control. The results presented in Figure 8.

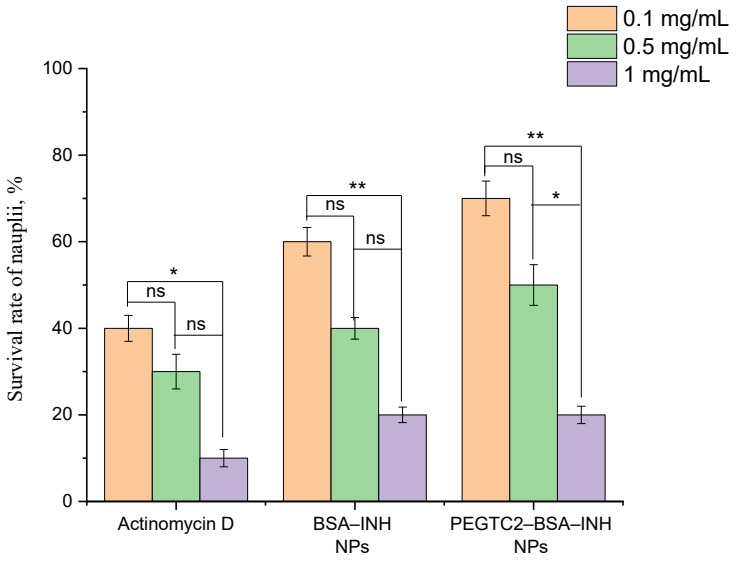

Figure 8. Survival rate of Artemia salina nauplii after 24-h exposure to actinomycin D, BSA–INH NPs and PEGTC2–BSA–INH NPs at the concentrations indicated. "*" indicates $p < 0.05$; "**" indicates $p < 0.01$; ns =not significant

The survival rate of nauplii decreased with increasing concentration for all samples studied, indicating a concentration-dependent toxic effect. At the highest concentration (1 mg/mL), actinomycin D exhibited the lowest survival rate, whilst the nanoparticles showed comparable survival rates. Overall, the PEGTC2–BSA–INH nanoparticles exhibited higher nauplii survival rates than the non-PEGylated BSA–INH nanoparticles at concentrations of 0.1 and 0.5 mg/mL, suggesting that PEGTC2 modification may improve the preliminary biocompatibility of the developed formulation. However, at a concentration of 1mg/mL, this difference was not observed, indicating that the potential protective effect of the PEGTC2 modification may be concentration-dependent. It has been established that nanoparticles exhibit lower toxicity than actinomycin D in relation to Artemia salina nauplii. Thus, this study using Artemia salina nauplii contributes to the growing literature on the biological effects of nanomaterials.

Polymer nanoparticles for drug delivery show great promise and are attracting considerable interest in the treatment of tuberculosis. Numerous studies have been conducted to encapsulate anti-tuberculosis drugs in various polymer carriers. Table 6 presents data from previously published studies on the isoniazid loaded nanoparticles.

Table 6

Comparison of the physicochemical characteristics and drug release behavior of INH-loaded polymeric nanoparticles reported in the literature

Nanoparticles	Size, nm	EE for INH, %	Drug release behavior	Reference
Human serum albumin	230±6 — 394±9	78±4 — 85±2	20 % of INH was released over a 24-hour	46
Chitosan-gellan gum	178±7	32	More than 20 % in 24 hours; an initial burst release followed by a sustained release	56
Mannosamine-Modified Poly(lactic-co-glycolic acid)-Polyethylene Glycol	117.67	5.85	Sustained drug release was achieved over a period exceeding 72 hour	57
Chitosan-INH	276.5	75.22	58.39 % INH released at 24 hour	58
Mannosylated chitosan-decorated PLGA	154.9 ± 21	79.8±0.45	Sustained drug release profile for 24 hour	59

Recent studies have investigated various polymeric nanocarriers for the delivery of isoniazid (INH), including systems based on chitosan, albumin, PLA and PLGA. Compared with these systems, the PEGTC2–BSA–INH nanoparticles developed in this study demonstrated high encapsulation efficiency, a mean particle size of 227 ± 1 nm and a narrow particle size distribution. The cumulative amount of INH released over 24 hours was approximately 2.3 mg. A preliminary toxicity assessment using Artemia salina nauplii showed higher survival rates with the PEGTC2–BSA–INH nanoparticles compared with the non-PEGylated BSA–INH nanoparticles at concentrations of 0.1 and 0.5mg/mL. Future studies will focus on evaluating the antimycobacterial activity and mucoadhesive properties of the developed nanoparticles with a view to further assessing their potential for delivering INH to the lungs in the treatment of tuberculosis.

Conclusions

In this study, isoniazid-loaded bovine serum albumin nanoparticles were successfully prepared using activated PEG (polyethylene glycol-dichloro-s-triazine). The production of PEGTC2–BSA–INH NPs was optimized using the Taguchi experimental design method. The optimal composition was obtained using activated PEG with a molecular weight of 6000 Da (20 mg/mL), BSA (40 mg/mL), and isoniazid (4 mg/mL) at pH 7, an ethanol addition rate of 1 mL/min, and a stirring speed of 200 rpm. The optimized PEGTC2–BSA–INH nanoparticles exhibited a controlled particle size of 227 ± 1 nm and a high encapsulation efficiency of 94 %, demonstrating efficient drug incorporation into the albumin-based carrier. SEM analysis revealed that the nanoparticles were predominantly spherical. In vitro release studies showed gradual and limited release of isoniazid, reaching approximately 2.3 mg after 24 h, indicating that most of the drug remained associated with the nanoparticles during the studied period. Overall, the developed PEGTC2–BSA–INH nanoparticles showed suitable physicochemical characteristics and warrant further investigation as a carrier for isoniazid delivery.

Supporting Information

The Supporting Information is available free at https://ejc.buketov.edu.kz/ejc/article/view/841/457

Funding

This work was supported by the Science Committee of the Ministry of Science and Higher Education of the Republic of Kazakhstan (Grant AP25794971) "Creation of PEGylated polymer nanosystems immobilized with anti-tuberculosis drug substances for the treatment of tuberculosis".

Acknowledgments

Yuliia Bardadym acknowledges the Research Council of Finland (No. 359456 for Ukrainian researchers) for her financial support.

The authors would like to express their sincere gratitude to Andrey Shibaev (BCMaterials — Basque Center for Materials, Applications and Nanostructures, Spain) for performing the ^{1}H and ^{13}C NMR measurements.

Declaration of Generative AI and AI-Assisted Technologies in the Writing Process

During the preparation of this work the authors used ChatGPT and Claude in order to improve the language and readability of the manuscript. After using this tools, the authors reviewed and edited the content as needed and take full responsibility for the content of the publication.

*Author Information**

**The authors' names are presented in the following order: First Name, Middle Name and Last Name*

Aldana Rymzhanovna Galiyeva (*corresponding author*) — PhD, Postdoctoral Researcher, Buketov Karaganda National Research University, Universitetskaya street, 28, 100024, Karaganda, Kazakhstan; e-mail: aldana_karaganda@mail.ru; https://orcid.org/0000-0002-8551-6297

Vladimir Olegovich Aseyev — PhD, Associate Professor, Department of Chemistry, University of Helsinki, Fabianinkatu 33, 00100, Helsinki, Finland; e-mail: vladimir.aseyev@helsinki.fi; https://orcid.org/0000-0002-0731-5254

Yuliia Volodymyrivna Bardadym — PhD, Department of Chemistry, University of Helsinki, Fabianinkatu 33, 00100, Helsinki, Finland; e-mail: yuliia.bardadym@helsinki.fi; https://orcid.org/0000-0002-9809-0897

Tolkyn Sergazyevna Zhumagaliyeva — Candidate of Chemical Sciences, Associate Professor, Buketov Karaganda National Research University, Universitetskaya street, 28, 100024, Karaganda, Kazakhstan; e-mail: zhumagalieva79@mail.ru; https://orcid.org/0000-0003-1765-752X

Askhat Sakenovich Borsynbayev — PhD, Senior Researcher of the LEP "Physical-chemical methods of investigation", Buketov Karaganda National Research University, Universitetskaya street, 28, 100024, Karaganda, Kazakhstan; e-mail: askhat.9@mail.ru; https://orcid.org/0000-0001-7709-5552

Yerkeblan Muratovich Tazhbayev — Professor, Doctor of Chemical Sciences, Buketov Karaganda National Research University, Universitetskaya street, 28, 100024, Karaganda, Kazakhstan; e-mail: tazhbaev@mail.ru; https://orcid.org/0000-0003-4828-2521

Author Contributions

The manuscript was written through contributions of all authors. All authors have given approval to the final version of the manuscript. CRediT: **Aldana Rymzhanovna Galiyeva** investigation, data curation, writing-original draft, funding acquisition; **Vladimir Olegovich Aseyev** investigation, resources, writing — review & editing; **Yuliia Bardadym Volodymyrivna** investigation; **Tolkyn Sergazyevna Zhumagaliyeva** data curation, formal analysis; **Askhat Sakenovich Borsynbayev** investigation; **Yerkeblan Muratovich Tazhbayev** conceptualization, writing — review & editing, visualization.

References

1 Global Tuberculosis Report 2025; World Health Organisation: Geneva, Switzerland, 2025

2 Cheung, S. -Y., Galiyeva, A., Tazhbayev, Y., Zhumagaliyeva, T., Bardadym, Y., & Aseyev, V. (2026). Mucoadhesive Chitosan–Gellan Gum Nanoparticles for Rifampicin Delivery: Taguchi Optimization and In Vitro Release Behavior. Pharmaceutics, 18(5), 627. https://doi.org/10.3390/pharmaceutics18050627

3 Omoteso, O. A., Fadaka, A. O., Walker, R. B., & Khamanga, S.M. Innovative Strategies for Combating Multidrug-Resistant Tuberculosis: Advances in Drug Delivery Systems and Treatment. Microorganisms, 2025, 13(4), 722. https://doi.org/10.3390/microorganisms13040722

4 Liebenberg, D., Gordhan, B. G., & Kana, B.D. Drug resistant tuberculosis: Implications for transmission, diagnosis, and disease management. Frontiers in Cellular and Infection Microbiology, 2022, 12. https://doi.org/10.3389/fcimb.2022.943545

5 Tazhbayev, Y.M., Galiyeva, A.R., Syrymova, U.Y., Zhaparova, L.Zh., Zhumagaliyeva, T.S. (2026). Rifampicin Loaded Chitosan-Based Nanoparticles: Optimization, Characterization, and Mucoadhesion. Eurasian Journal of Chemistry, 31, 1(121), 45–60. https://doi.org/10.31489/2959-0663/1-26-4

6 Tanjung, Y., Dewi, M., Gatera, V., Barliana, M., Joni, I. M., & Chaerunisaa, A. (2024). Factors Affecting the Synthesis of Bovine Serum Albumin Nanoparticles Using the Desolvation Method. Nanotechnology, Sci. Appl., Volume 17, 21–40. https://doi.org/10.2147/nsa.s441324

7 Kouchakzadeh, H., Safavi, M. S., & Shojaosadati, S. A. (2015). Efficient Delivery of Therapeutic Agents by Using Targeted Albumin Nanoparticles. Protein and Peptide Nanoparticles for Drug Delivery, 121–143. https://doi.org/10.1016/bs.apcsb.2014.11.002

8 Galisteo-González, F., & Molina-Bolívar, J. A. (2014). Systematic study on the preparation of BSA nanoparticles. Colloids and Surfaces B: Biointerfaces, 123, 286–292. https://doi.org/10.1016/j.colsurfb.2014.09.028

9 Srivastava, A., & Prajapati, A. (2020). Albumin and functionalized albumin nanoparticles: production strategies, characterization, and target indications. Asian Biomedicine, 14(6), 217–242. https://doi.org/10.1515/abm-2020-0032

10 Kiarashi, M., & Yasamineh, S. (2024). Albumin nanoparticles are a promising drug delivery system in dentistry. BioMedical Engineering OnLine, 23(1). https://doi.org/10.1186/s12938-024-01318-9

11 Pérez-Herrero, E., Fernández-Medarde, A., & Irache, J. M. (2026). Albumin-based nanocarriers: Singularities, synthesis methods, clinical relevance and targeting strategies in cancer. Acta Pharmaceutica Sinica B, 16(4), 1883–1913. https://doi.org/10.1016/j.apsb.2025.11.035

12 Folda, P., Weidinger, E., Seidl, J., Yazdi, M., Pöhmerer, J., Grau, M., Minde, D. P., Ali, M., Kimna, C., & Wagner, E. (2025). PEGylation Enhances Colloidal Stability and Promotes Ligand-Mediated Targeting of LAF–Xenopeptide mRNA Complexes. Polymers, 17(22), 2979. https://doi.org/10.3390/polym17222979

13 Suk, J. S., Xu, Q., Kim, N., Hanes, J., & Ensign, L. M. (2016). PEGylation as a strategy for improving nanoparticle-based drug and gene delivery. Advanced Drug Delivery Reviews, 99, 28–51. https://doi.org/10.1016/j.addr.2015.09.012

14 Gao, P. (2025). PEGylated lipids in lipid nanoparticle delivery dynamics and therapeutic innovation. Beilstein Journal of Nanotechnology, 16, 1914–1930. Portico. https://doi.org/10.3762/bjnano.16.133

15 Calvopiña, J., Irache, J. M., Martínez-Oharriz, M. C., Palacio, J. F., Galindo, J. I. A., Górriz, F. J., & Rivero, P. J. (2026). Effect of PEG molecular weight on the physicochemical properties of zein nanoparticles: A comparative study. International Journal of Biological Macromolecules, 382, 154366. https://doi.org/10.1016/j.ijbiomac.2026.154366

16 Galiyeva, A. R., Tazhbayev, Y. M., Yessentayeva, N. A., Daribay, A. T., Marsel, D. T., Sadyrbekov, D. T., Zhaparova, L. Zh., & Arystanova, Z. T. (2023). PEGylation of Albumin Nanoparticles Immobilized with the Anti-Tuberculosis Drug "Isoniazid". Eurasian Journal of Chemistry, 28(2 (110)). https://doi.org/10.31489/2959-0663/2-23-7

17 El-Faham, A., Al-Rasheed, H. H., Sholkamy, E. N., Osman, S. M., & Alothman, Z. A. (2020). Simple Approaches for the Synthesis of AgNPs in Solution and Solid Phase Using Modified Methoxypolyethylene Glycol and Evaluation of Their Antimicrobial Activity. International Journal of Nanomedicine, 15, 2353-2362. https://doi.org/10.2147/ijn.s244678

18 Abuchowski, A., van Es, T., Palczuk, N. C., & Davis, F. F. (1977). Alteration of immunological properties of bovine serum albumin by covalent attachment of polyethylene glycol. Journal of Biological Chemistry, 252(11), 3578–3581. https://doi.org/10.1016/s0021-9258(17)40291-2

19 Dąbkowska, M., Kosiorowska-Kraj, A., Szatanik, A., Filip, K., Martínez-Orts, M., Pujals, S., Olszewska, M., & Pukacka, K. (2026). Tunable PEGylated albumin nanocarriers enhance 5-FU cytotoxic selectivity and modulate oxidative and immune stress in colorectal cancer model. Biomedicine &Amp; Pharmacotherapy, 196, 118958. https://doi.org/10.1016/j.biopha.2025.118958

20 Galiyeva, A. R., Tazhbayev, Ye. M., Zhumagaliyeva, T. S., Sadyrbekov, D. T., Kaikenov, D. A., Karimova, B. N., Shokenova, S. S., &. (2022). Polylactide-co-glycolide nanoparticles immobilized with isoniazid: optimization using the experimental Taguchi method. Bulletin of the Karaganda University. "Chemistry" Series, 105(1), 69–77. https://doi.org/10.31489/2022ch1/69-77

21 Masoud, A., Hosseini, S. M. S., Dini, A., & Kamyabi, M. (2026). Taguchi-based multi-response optimization of lead flotation from a complex Zn–Pb sulfide ore. Scientific Reports. https://doi.org/10.1038/s41598-026-68892-x

22 Gupta, R., Sarkar, M., & Xie, H. (2026). From Screening to Optimization: Strategic Implementation of Design of Experiments (DOE) for Robust Nanoparticle Formulation. Polymers, 18(16), 2034. https://doi.org/10.3390/polym18162034

23 Kimura, K., Yamasaki, K., Nakamura, H., Haratake, M., Taguchi, K., & Otagiri, M. (2018). Preparation and in Vitro Analysis of Human Serum Albumin Nanoparticles Loaded with Anthracycline Derivatives. Chemical and Pharmaceutical Bulletin, 66(4), 382–390. https://doi.org/10.1248/cpb.c17-00838

24 Aukunuru, J., Thadakapally, R., Aafreen, A., Habibuddin, M., & Jogala, S. (2016). Preparation and characterization of PEG-albumin-curcumin nanoparticles intended to treat breast cancer. Indian Journal of Pharmaceutical Sciences, 78(1), 65. https://doi.org/10.4103/0250-474x.180250

25 Gao, Y., Joshi, M., Zhao, Z., & Mitragotri, S. (2023). PEGylated therapeutics in the clinic. Bioengineering &Amp; Translational Medicine, 9(1). Portico. https://doi.org/10.1002/btm2.10600

26 Lee, C. S., Kulkarni, Y., Pierre, V., Maski, M., & Wanner, C. (2024). Adverse Impacts of PEGylated Protein Therapeutics: A Targeted Literature Review. BioDrugs, 38(6), 795–819. https://doi.org/10.1007/s40259-024-00684-z

27 Porfiryeva, N. N., Moustafine, R. I., & Khutoryanskiy, V. V. (2020). PEGylated Systems in Pharmaceutics. Polymer Science, Series C, 62(1), 62–74. https://doi.org/10.1134/s181123822001004x

28 Tekade, R. K., & Chougule, M. B. (2013). Formulation Development and Evaluation of Hybrid Nanocarrier for Cancer Therapy: Taguchi Orthogonal Array Based Design. BioMed Research International, 2013, 1–18. https://doi.org/10.1155/2013/712678

29 Kunda, N. K., Alfagih, I. M., Dennison, S. R., Tawfeek, H. M., Somavarapu, S., Hutcheon, G. A., & Saleem, I. Y. (2014). Bovine Serum Albumin Adsorbed PGA-co-PDL Nanocarriers for Vaccine Delivery via Dry Powder Inhalation. Pharmaceutical Research, 32(4), 1341–1353. https://doi.org/10.1007/s11095-014-1538-5

30 Villani, E., Stagno, V., Maiuro, A., Travisano, G., & Capuani, S. (2026). Multi-parametric high-resolution MRI for the characterisation of water and PEG solutions in wood. European Journal of Wood and Wood Products, 84(2). https://doi.org/10.1007/s00107-026-02388-3

31 Hoz A, Sánchez-Migallón A. Green synthesis of 1,3,5-triazines with applications in supramolecular and materials chemistry. Targets in Heterocyclic Systems. 2017; 20: 139-173. http://dx.medra.org/10.17374/targets.2017.20.139

32 Fulmer, G. R., Miller, A. J. M., Sherden, N. H., Gottlieb, H. E., Nudelman, A., Stoltz, B. M., Bercaw, J. E., & Goldberg, K. I. (2010). NMR Chemical Shifts of Trace Impurities: Common Laboratory Solvents, Organics, and Gases in Deuterated Solvents Relevant to the Organometallic Chemist. Organometallics, 29(9), 2176–2179. https://doi.org/10.1021/om100106e

33 Costa, A., Pinheiro, M., Magalhães, J., Ribeiro, R., Seabra, V., Reis, S., & Sarmento, B. (2016). The formulation of nanomedicines for treating tuberculosis. Advanced Drug Delivery Reviews, 102, 102–115. https://doi.org/10.1016/j.addr.2016.04.012

34 Tazhbayev, Y.; Mukashev, O.; Burkeyev, M.; Lozinsky, V.I. Synthesis and Comparative Study of Nanoparticles Derived from Bovine and Human Serum Albumins. Polymers 2020, 12, 1301. https://doi.org/10.3390/polym12061301

35 Zhang, T., Guo, X., Meng, H., Tang, X., Ai, C., Chen, H., Lin, J., & Yu, S. (2020). Effects of bovine serum albumin on the ethanol precipitation of sugar beet pulp pectins. Food Hydrocolloids, 105, 105813. https://doi.org/10.1016/j.foodhyd.2020.105813

36 Yan, L., Reid, E., Chen, Z., He, J., & Chen, Y. (2026). Rapid, High-Capacity, and Reusable Bovine Serum Albumin-Based Adsorbents for Perfluoroalkyl and Polyfluoroalkyl Substance Removal. ACS Applied Materials &Amp; Interfaces, 18(3), 5026–5037. https://doi.org/10.1021/acsami.5c13467

37 Bhattacharjee, S. (2016). DLS and zeta potential — What they are and what they are not? Journal of Controlled Release, 235, 337–351. https://doi.org/10.1016/j.jconrel.2016.06.017

38 Lowry, G. V., Hill, R. J., Harper, S., Rawle, A. F., Hendren, C. O., Klaessig, F., Nobbmann, U., Sayre, P., & Rumble, J. (2016). Guidance to improve the scientific value of zeta-potential measurements in nanoEHS. Environmental Science: Nano, 3(5), 953–965. https://doi.org/10.1039/c6en00136j

39 Givens, B. E., Diklich, N. D., Fiegel, J., & Grassian, V. H. (2017). Adsorption of bovine serum albumin on silicon dioxide nanoparticles: Impact of pH on nanoparticle–protein interactions. Biointerphases, 12(2). https://doi.org/10.1116/1.4982598

40 Pham, D. -D., Fattal, E., & Tsapis, N. (2015). Pyrazinamide-loaded poly(lactide-co-glycolide) nanoparticles: Optimization by experimental design. Journal of Drug Delivery Science and Technology, 30, 384–390. https://doi.org/10.1016/j.jddst.2015.07.006

41 Xie, G., Lu, Y., Lu, X., Zhang, Z., & Lin, S. (2025). Measurement Error Analysis and Thermal Degradation Kinetic Model Improvement for Thermogravimetric Analyzers. Polymers, 17(17), 2390. https://doi.org/10.3390/polym17172390

42 Gibson, R. L., Simmons, M. J. H., Stitt, E. H., Horsburgh, L., & Gallen, R. W. (2021). Selection of Formal Baseline Correction Methods in Thermal Analysis. Chemical Engineering &Amp; Technology, 45(2), 238–248. Portico. https://doi.org/10.1002/ceat.202100120

43 Crewe, R. J., Staggs, J. E. J., & Williams, P. T. (2007). Drag-induced apparent mass gain in thermogravimetry. Polymer Degradation and Stability, 92(11), 2070–2075. https://doi.org/10.1016/j.polymdegradstab.2007.07.023

44 Galiyeva, A.R., Tazhbayev, Ye.M., Zhumagaliyeva, T.S., & Daribay, A.T. (2022) Encapsulation of Isoniazid in Polylactide-Co-Glycolide Nanoparticles by Nanoprecipitation. Bulletin of the University of Karaganda — Chemistry, 107(3), 208-217. https://doi.org/10.31489/2022Ch3/3-22-17

45 Vilela Tibola, A. P. O., & Carpentieri Rodrigues, L. N. (2017). Compatibility study between isoniazid and pharmaceutical excipients used in solid dosage forms. International Research Journal of Pharmacy, 7(12), 18–22. https://doi.org/10.7897/2230-8407.0712140

46 Galiyeva, A., Tazhbayev, Y., Zhumagaliyeva, T., Karimova, B., Tabriz, N., & Khutoryanskiy, V. V. (2025). Synthesis and Investigation of Albumin Nanoparticles Loaded With Anti-Tuberculosis Drug Isoniazid. Biopolymers, 116(4). Portico. https://doi.org/10.1002/bip.70036

47 Adamiano, A., Lesci, I. G., Fabbri, D., & Roveri, N. (2015). Adsorption of bovine serum albumin onto synthetic Fe-doped geomimetic chrysotile. Journal of the Royal Society, Interface, 12(107), 20150186. https://doi.org/10.1098/rsif.2015.0186

48 Michnik, A., Michalik, K., Kluczewska, A., & Drzazga, Z. (2006). Comparative DSC study of human and bovine serum albumin. Journal of Thermal Analysis and Calorimetry, 84(1), 113–117. https://doi.org/10.1007/s10973-005-7170-1

49 Galiyeva, A. R., Yessentayeva, N. A., Marsel, D. T., Daribay, A. T., Sadyrbekov, D. T., Moustafine, R. I., & Kutulutskaya, T. V. (2025). Polylactide Acid-Based Nanoparticles for Controlled Delivery of Isoniazid and Rifampicin: Synthesis, Characterization, and In Vitro Release Study. Eurasian Journal of Chemistry, 30(2(118)), 95–108. https://doi.org/10.31489/2959-0663/2-25-12

50 Yessentayeva, N. A., Galiyeva, A. R., Daribay, A. T., Sadyrbekov, D. T., Zhumagalieva, T. S., & Marsel, D. T. (2024). Synthesis and Optimization of Bovine Serum Albumin Nanoparticles Immobilized with Antituberculosis Drugs. Eurasian Journal of Chemistry. https://doi.org/10.31489/2959-0663/1-24-6

51 Askari, F., Zandi, M., Shokrolahi, P., Tabatabaei, M. H., & Hajirasoliha, E. (2019). Reduction in protein absorption on ophthalmic lenses by PEGDA bulk modification of silicone acrylate-based formulation. Progress in Biomaterials, 8(3), 169–183. https://doi.org/10.1007/s40204-019-00119-x

52 Jin, G., Jin, M., Jin, Z., Gao, Z., & Yin, X. (2016). Docetaxel-loaded PEG-albumin nanoparticles with improved antitumor efficiency against non-small cell lung cancer. Oncology Reports, 36(2), 871–876. https://doi.org/10.3892/or.2016.4863

53 Santos, J. H. P. M., Torres-Obreque, K. M., Meneguetti, G. P., Amaro, B. P., & Rangel-Yagui, C. O. (2018). Protein PEGylation for the design of biobetters: from reaction to purification processes. Brazilian Journal of Pharmaceutical Sciences, 54(spe). https://doi.org/10.1590/s2175-97902018000001009

54 Casettari, L., Vllasaliu, D., Mantovani, G., Howdle, S. M., Stolnik, S., & Illum, L. (2010). Effect of PEGylation on the Toxicity and Permeability Enhancement of Chitosan. Biomacromolecules, 11(11), 2854–2865. https://doi.org/10.1021/bm100522c

55 Hu, J., & Liu, S. (2022). Emerging trends of discrete Poly(ethylene glycol) in biomedical applications. Current Opinion in Biomedical Engineering, 24, 100419. https://doi.org/10.1016/j.cobme.2022.100419

56 Tazhbayev, Y., Cheung, S. -Y., Galiyeva, A., Slouf, M., Kostka, L., Zhumagaliyeva, T., Zhaparova, L., Daribay, A., & Kaziyev, A. (2026). Chitosan-Gellan Gum Nanoparticles for Antituberculosis Drug Encapsulation: Synthesis, Characterization and In Vitro Investigation. Polymers, 18(17), 2139. https://doi.org/10.3390/polym18172139

57 Peng, C., Luan, H., Shang, Q., Xiang, W., Yasin, P., & Song, X. (2025). Mannosamine-Modified Poly(lactic-co-glycolic acid)-Polyethylene Glycol Nanoparticles for the Targeted Delivery of Rifapentine and Isoniazid in Tuberculosis Therapy. Bioconjugate Chemistry, 36(5), 1021–1033. https://doi.org/10.1021/acs.bioconjchem.5c00062

58 Sanju, S.K. Singh, Prashant Purohit, Tejaram, & Kashi Ram. (2024). Preparation and Characterization of Isoniazid Loaded Nanoparticles Using Natural Polymers. International Journal of Pharma and Bio Sciences, 31–39. https://doi.org/10.22376/ijpbs.2024.15.2.p31-39

59 Maqbool, R., Nayab, D. E., Mubeen, M., Ali, H., & Khan, S. (2025). Mannosylated chitosan-decorated PLGA nanoparticles for targeted pulmonary delivery of isoniazid: a promising approach in the treatment of tuberculosis. Journal of Drug Targeting, 34(2), 301–314. https://doi.org/10.1080/1061186x.2025.2554761